Self-Tuning Controller-Based Optimization of Fixed-Wing UAV Attitude Control

*1S. Meenakshi, 2G. Prabhakar, 3S. Selvaperumal

*1Research scholar, Department of Electronics and Communication Engineering, Thiagarajar College of Engineering, Madurai, Tamilnadu, India.

² Assistant Professor, Department of Electronics and Communication Engineering, Thiagarajar College of Engineering, Madurai, Tamilnadu, India.

³Professor/Department of Electrical and Electronics Engineering, NPR College of Engineering and Technology (Autonomous), Natham- 624 401, Dindigul, Tamil Nadu, India.

Abstract: Controllers are used in this low-cost fixed-wing unmanned aerial vehicle. We adapted the system by employing the inner and outer loop design techniques. The navigation and stabilization systems each have two external loops, which are used to maintain track of the trajectory and alter the attitude. A technique called Model Reference Adaptive Control (MRAC) design and a technique called self-tuning controller design are two approaches for creating adaptive controllers, respectively. This article describes an EVTOL UAV controller that can be used in all flight modes, including hover, cruise and partially transitioned. When flying at low to moderate speeds, a wide range of pitch angles can be used for trajectory tracking, as we demonstrate in this section. We can freely change the vehicle's pitch in order to reduce the vehicle's thrust as well as its energy consumption. For the vehicle to operate in a wide range of airspeeds, flight paths, and angles of attack, geometric attitude control and airspeed-dependent control allocation algorithms are used in combination.

Keywords: PID; Fuzzy Logic Controller; Model Reference Adaptive Control; Unmanned Aerial Vehicle

. INTRODUCTION

Fixed-wing UAVs have a stiff wing with a specified air foil that generates lift due to the aircraft's forward speed, allowing it to take off and land. Changing the angle of attack causes the lift to alter. To ascend, gliding fixed-wing aircraft rely on air movement, whereas powered fixed-wing aircraft use propulsion to propel themselves upward. The term "airframe" refers to the plane's structural components. There are three parts to an aircraft's airframe: the wing, the fuselage, and the landing gear (Visintini et al., 2021). The three axes of flight rotation (pitch, roll, and yaw) are crucial for constructing an aircraft (P. Chen, 2021). During steady-state flight, the aircraft's centre of gravity, or cg, rotates at these specific angles. The term "roll" refers to the rotation of the vehicle in relation to its longitudinal axis. The equilibrium roll angle is the angle at which the plane's wings are parallel to the ground. During steady-state flight, the dihedral wings of a fixed-wing aircraft offer roll stability to prevent the aircraft from dipping its wings. The aircraft's vertical body axis acts as the yaw axis (Xue et al., 2021). Yaw stability is provided by a vertical stabilizer (or fin) attached to a plane's wing at the back. Finally, pitch is the rotation about the axis perpendicular to the longitudinal plane of symmetry, which is the rotation about pitch. The aircraft's pitch is controlled by the horizontal stabilizer, which is similarly located at the rear (Bornebusch et al., 2021). A fixedwing aircraft's pitching moment directly correlates to the angle of attack measure that affects lift, as depicted in Fig.1. Aircraft nose up during take-off increases the angle of attack. The aircraft's speed will be considerably slowed if the pitch is too high, resulting in a stall pattern. As previous work, the stability of a rotor wing is based on three factors: pitch, roll, and yaw. The rotors provide variable amounts of power and torque, which are used to control the UAV. The nose-down flight pattern of the multi-rotor UAV is generated as a result of the fact that the back rotors provide more thrust than the front (Lee et al., 2021). Because the rotor torque is stronger in the diagonal rotors than in the counter rotors, the yaw rotation axis for movement is not balanced. The yaw and roll axes of a fixed-wing aircraft are entangled with one another.



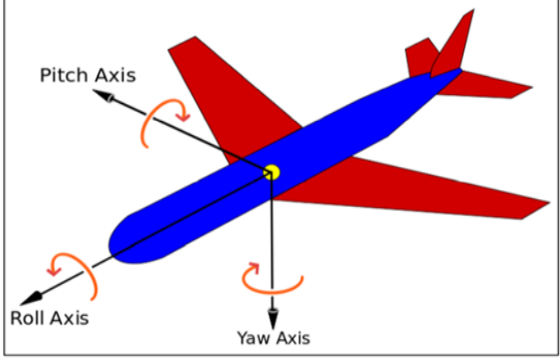


Figure. 1. Flight angle of rotation

When it comes to rotary-wing aircraft, yaw and roll are regarded to be one lateral movement combined (Umamaheswari et al., 2021). Rotor-wing aircraft are projected to have half the endurance of fixed-wing aircraft if they have a reasonable L/D ratio and the same weight as fixed-wing aircraft (Zhang et al., 2021). The vehicle's endurance is diminished as a result of the additional power required to generate push through the use of rotors. Using remote controllers or pre-programmed controls, unmanned rotary-wing aircraft can be flown from the ground using remote controls. Modeling the UAV dynamics is achieved using a component build-up method. The aerodynamic coefficients and aircraft rigid body equations of motion in order to determine unmanned aerial vehicle (UAV) translational, angular, and attitude (roll, pitch, and yaw angles) and inertial position is shown in Fig.2 (Liu et al., 2021). Although the dynamics of an unmanned aerial vehicle (UAV) are substantially more complex, the equations of motion (1) - (18) can be utilized to approximate flight dynamics.

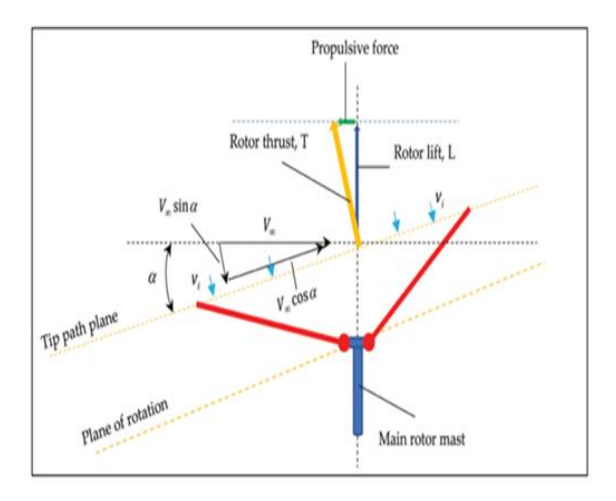


Figure. 2. Aerodynamic parameter on rotor in flights

$$A = \frac{b^2}{S} \tag{1}$$

$$L = C_L(\frac{\rho}{2}) X V^2 X S \tag{2}$$

$$D = C_D(\frac{\rho}{2}) X V^2 X S$$
 (3)

$$C_{L} = \left(\frac{W}{S}\right) \left(\frac{2}{\rho}\right) \left(\frac{1}{V^2}\right) \tag{4}$$

$$C_D = C_{D0} + C_{Di} = C_{D0} + (K \times C_L^2)$$
 (5)

$$K = \frac{1}{\pi x A x e} \tag{6}$$

Aircraft, sensor, guidance command generator, and controllers are all components of a collision avoidance system

depicted in the diagram displayed in Fig.3. Modeling non-linear 6-DOF UAV dynamics in a simulation environment using flight dynamics equations of motion allows us to extract UAV states using a middle-sized fixed wing UAV model (Qiu et al., 2020).

Force equation

$$F_{x} = m(\dot{U} + qW - Vr) \tag{7}$$

$$F_{v} = m(\dot{V} + PW - Ur) \tag{8}$$

$$F_z = m(\dot{W} + pW - Uq) \tag{9}$$

Moment equation

$$M_X = I_{XX} \dot{p} - I_{Xz} (\dot{r} + pq) + (I_{zz} - I_{yy}) qr \qquad (10)$$

$$M_{y} = I_{yy}\dot{q} - I_{Xz}(p^{2} + r^{2}) + (I_{xx} - I_{zz})pr$$
 (11)

$$M_Z = I_{zz}\dot{r} - I_{Xz}\dot{p} + pq(I_{xx} - I_{zz}) + I_{Xz}qr$$
 (12)

Kinematic equation

$$\dot{\mathbf{Q}} = p + \tan\theta \left(q \sin\varphi + r\cos\varphi \right) \tag{13}$$

$$\dot{\theta} = q\cos\varphi - r\sin\varphi \tag{14}$$

$$\dot{\bigcup} = q \sin \varphi \sec \theta + r \cos \varphi \sec \theta \tag{15}$$

$$\dot{P}_n = U\cos\theta\cos\varphi + V(-\cos\varphi\sin\psi + \sin\varphi\sin\theta\cos\psi)$$

$$\sin \varphi \sin \theta \cos \psi) + W(\cos \varphi \cos \psi + (16))$$

$$\dot{P}_e = U\cos\theta\sin\varphi + V(\cos\varphi\cos\psi + \cos\varphi\sin\theta\sin\psi)$$

$$\sin \varphi \sin \theta \sin \psi) + W(-\sin \varphi \cos \psi + (17))$$

 $\dot{h} = U \sin \theta - V(\cos \varphi \sin \psi + \sin \varphi \cos \theta)$

 $+W(\cos\varphi\cos\theta)$

(18)

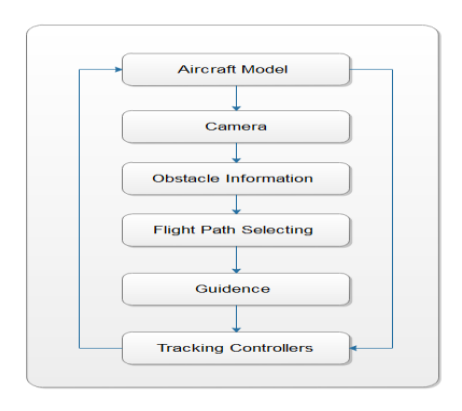


Figure. 3. Collision avoidance system flow diagram

2. BACKGRROUND

2.1 PID Controller:

Non-linear dynamic models can be linearized around defined trimming points and regarded simple SISO or MIMO linear systems, therefore the cascaded PID controller can be used for UAV flight control. UAV dynamics can be controlled in two ways: longitudinally and laterally. The autopilot's capacity to keep track of the flying route is crucial (Borup et al., 2020). With an unmanned aerial vehicle (UAV), search and rescue missions can be carried out on their own. Thus, the capacity to keep track of the UAV's path is essential to its effective search.

Navigation control can be broken down into longitudinal and lateral control, as shown in Fig.4 and the corresponding equations are represented as (19), (20) and (21).

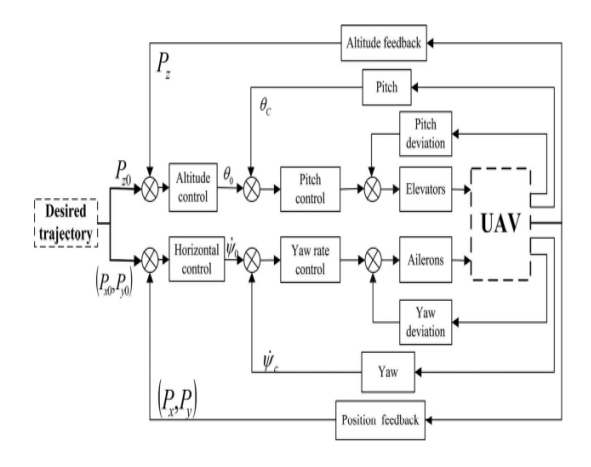


Figure. 4. Block Diagram of PID controller

$$\delta_{a}(t) = K_{c}^{p}(p^{*}-p) + \frac{K_{c}^{p}}{\tau_{l}^{p}} \int_{0}^{t} (p^{*}(\tau) - p(\tau)) d\tau$$
 (19)

$$\delta_{e}(t) = K_{c}^{q}(q^{*}-q) + \frac{K_{c}^{q}}{\tau_{l}^{q}} \int_{0}^{t} (q^{*}(\tau) - q(\tau)) d\tau$$
 (20)

$$\delta_{r}(t) = K_{c}^{r}(r^{*}-r) + \frac{K_{c}^{r}}{\tau_{l}^{r}} \int_{0}^{t} (r^{*}(\tau) - r(\tau)) d\tau$$
 (21)

2.2 Fuzzy logic system:

Fuzzy logic is used to create Fuzzy Inference Systems. Defining the mapping between an input and an output is known as fuzzy inference (Song et al., 2020). A Fuzzy Logic System or a Fuzzy Inference System translates the inputs into the outputs in a way that is consistent (Ramamoorthy et al., 2022). The rule-base, data-base, fuzzifier, inference, and defuzzifier are all included. The major purpose of the proposed method is to find a path for the UAV that is free of collisions in dynamic barriers. Multi-objective constraints are used to identify the blockages in UAV networks, which are then removed from the network. Figure 5 illustrates how an enhanced dynamic obstacle avoidance strategy can be used to solve the issues associated with UAV path planning and selection by using the weighted least squares and sequential least square optimization. Weighted least squares coefficient estimates are frequently close to unweight values. If they are significantly different, the technique can be repeated until the estimated coefficients settle (usually in one or two iterations). The weights may be based on theory or prior study in some circumstances. When using large replicates, weights can be computed directly from sample variances of the response variable for each predictor variable combination. Weighting will (legitimately) affect statistical interval widths. The least squares model becomes quadratic optimization. Sequential quadratic programming can then find the optimal solution once the iterative point enters the feasible region.

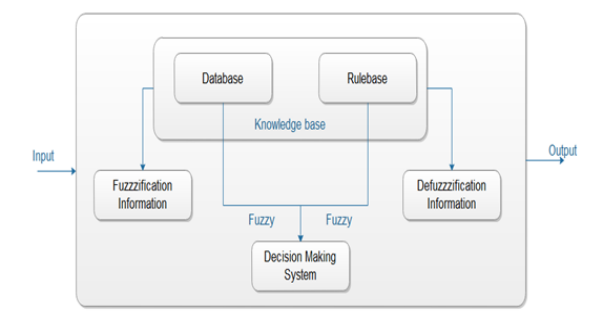


Figure. 5. Fuzzy interface system

Vol. 46 No. 1 (2025)

3. PROPOSED WORK

There are a lot of options available to the Nederdrone when it comes to entering a new state. Consider how the actuators will be controlled in the event that there are more actuators than are required to attain the desired state. Propellers or elevons, for example, can be used to change the pitch angle of the aircraft (Borup et al., 2020). The positioning of actuators is discussed in detail in this portion of the study. Control allocation can help to alleviate saturation, which has also been shown in the literature. It is feasible to resolve these concerns using a variety of tactics, including the weighted least squares and sequential least squares optimization techniques, which are also discussed below. Using a graphical representation, Figure 6 illustrates the problem of control allocation. As a result, it will translate the virtual input (v(t)) of the controller into the input required by the UAV controller. The following factors limit u's options: $u \le u \le \neg u$.

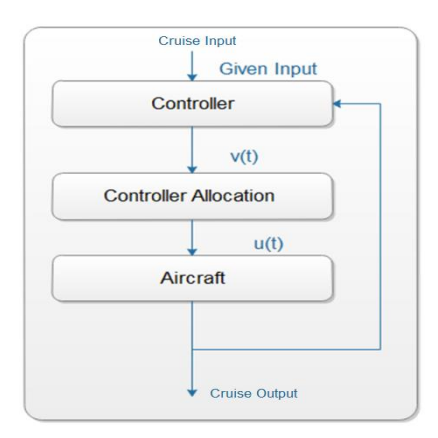


Figure. 6. Block diagram of control allocation

Where u and ~u are the upper and lower bounds of the necessary input, respectively. If the inputs are correct, optimization will provide the most efficient path possible. If the goal is to reach the new state as rapidly as possible, weight factors could be used to achieve this goal (Liu et al., 2020). For example, if a UAV's attitude cannot be optimized to match the needs of a certain virtual input, the UAV should be replaced. The online trajectory generator, as depicted in Figure 7, starts with the current state information as an initial condition and then generates a new best trajectory by combining the pseudo spectral approach with the existing obstacle data to produce the best possible route. Following that, the autopilot is given the order to continue this course (Mitikiri et al., 2019).

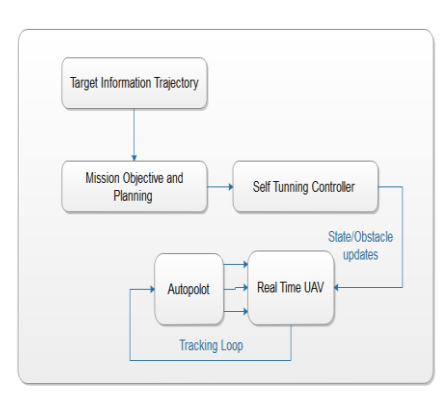


Figure. 7. Proposed block diagram for fixed wing UAV

A new state or obstacle is discovered and the optimal path is computed each time it is discovered. This allows the system to survive changes in obstacle information as well as the effects of the unmanned aerial vehicle. Given the limited amount of time available for each fresh trajectory computation, the trajectory command sent to the autopilot is based on the trajectory computed using state information from a previous sample time and delivered to the autopilot. With the help of this predictive technique, it is possible to adjust for process delays (Mobarez, et al., 2019). As previously stated, there is no connection between the axes of the launch vehicle's pitch, yaw, and roll in the preceding section. Because of the vehicle's elevated altitude above the atmosphere, this type of launch

vehicle has two aerodynamic effects, and the parameters are sluggish to change in nature (Tang et al., 2019). As such, a linear controller with a predetermined gain schedule is sufficient to stabilize and regulate the vehicle throughout its operational range.

There are two ways for creating adaptive controllers: the model reference adaptive control (MRAC) design methodology and the self-tuning Controller approach. When using the MRAC technique, a reference model is created, and an adaptation algorithm is used to modify the controller gains so that they are consistent with the reference model's (H. Wang, 2019). To put it another way, a controller can be self-tuning if it has the ability to alter its own settings, as described by Kalman and colleagues in their study. Having a launch vehicle factory on hand allows for the implementation of the self-tuning controller technique if the plant characteristics are known with sufficient accuracy. The structure contains two different loops that function as a controller. 1. A traditional controller with variable parameters in an inner loop and 2. An outer loop of an identifier and design box, which alters these controller parameters, is also included. When it comes to selecting a controller design methodology and an identification system, the self-tuning regulator is quite adaptable. The representative block diagram of a self-tuning controller is given in the Fig. 8.

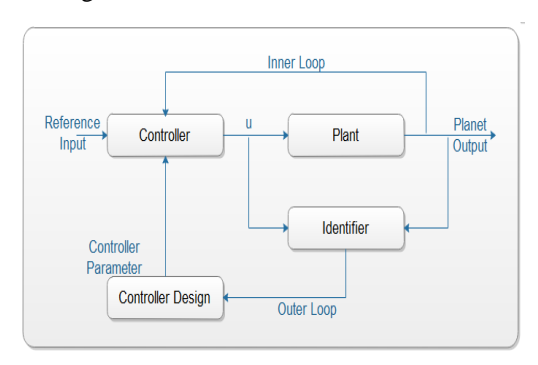


Figure. 8. Block diagram of self-tuning controller

4. TRAJECTORY TRACKING SYSTEM

The tracking of multi-rotor unmanned aerial vehicles (UAVs) has been extensively studied, and it serves as the foundation for the study given here. As a result of its better tracking performance, geometric control (Yang et al., 2019) is commonly used for multi-rotor control. The differentially flat (Tang et al., 2019) yaw trajectory of multi-rotors, combined with under-actuated dynamics, is used to create feed-forward thrust and attitude commands from a position trajectory that differs by three times and a yaw trajectory that differs by one time. This control system employs proportional-derivative feedback control in order to attain the desired trajectory. The flowchart of a trajectory tracking system is shown in Fig. 9.

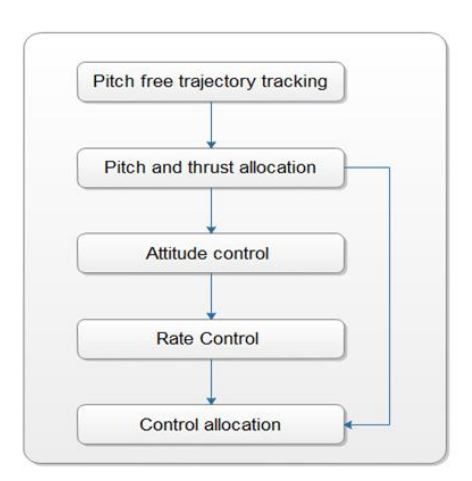


Figure. 9. Trajectory tracking system – flow diagram

Attack angles that are too high when switching between VTOL and fixed-wing flight might alter the

behaviour of a winged electric vertical take-off and landing vehicle (eVTOL), leading to stallingand unstable aerodynamics. The majority of proposed control methods for winged eVTOLs differ in the manner in which the transition is governed as a result of their design. The use of incremental nonlinear dynamic inversion and gain scheduling based on empirical data (Poksawat et al., 2019) has been demonstrated to be effective in stabilizing human-piloted winged eVTOL aircraft. A multirotor and a fixed-wing controller's input is combined during the transition period1 of the Ardunio flight controller's transition period (Fusini et al., 2018). Using this technique, hovering and flying with a fixed wing are both conceivable, but there are no other flight modes that can be controlled. For control of the UAV, it was essential to reproduce imagery that would be captured by a sensor attached to the UAV. This was done in order to provide visual input for control. The approach for creating data was derived from the concept of projecting key points in the simulated environment (for example, electricity poles) from the ground to the image plane of a sensor (Zhengi et al., 2017). These points could be linked together within the image in order to produce a simulated view of the feature.

5. RESULT

It is shown in this Fig.11, what happens when you change the flight path angles while keeping the velocity and target power constant at $V_a = 3.0$ m/s. Following a pitch allocation of 15^0 , there is an increase. It can be seen here how the pitch angle reaches its maximum and how the thrust compensates for a lack of lift while the plane is flying at a low airspeed in this diagram. The vehicle's wings create enough lift after $V_a = 10$ m/s is reached, that it no longer requires z p propulsion. As a result, there has been a complete metamorphosis. Fig. 10 depicts a change in force direction that does not influence the flight path or speeds of the aircraft. An increase in total thrust happens above this threshold when the multirotor method continues to pitch forward while the optimized techniques stay at maximum and continue to produce thrust utilizing Tx while the multirotor method remains at maximum. In the figure 10 and 11 Optimal thrust and pitch for increasing flight path angles are shown in terms of Small Angle (SA), Flat Plate (FP) and Blended 2 (B2).

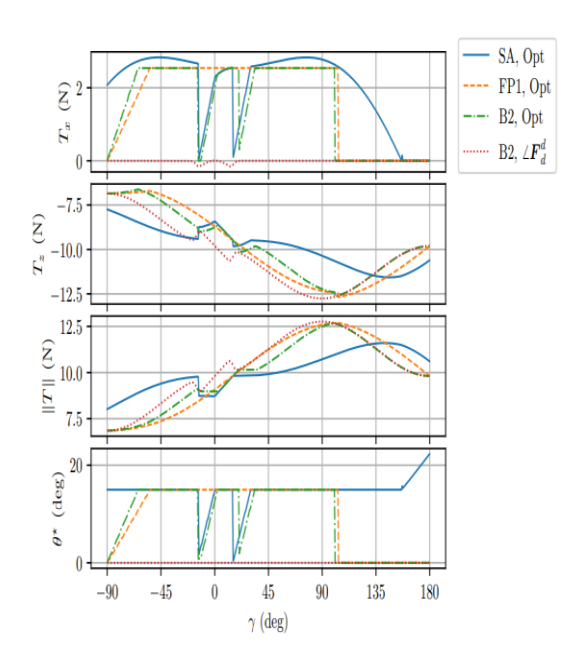


Figure. 10. Optimal thrust and pitch for increasing flight path angles

There are many possible flight paths, and each one is designed to accommodate a variety of scenarios, from takeoff to landing to a yaw maneuver. It is important to note that the waypoints in Table 1 are identical to those shown in Figs 10 and 11 for the sake of the trajectories. There are two sets of data shown in Figure 12 the yaw and position pathways as well as the position error, thrust magnitude, and pitch angle.

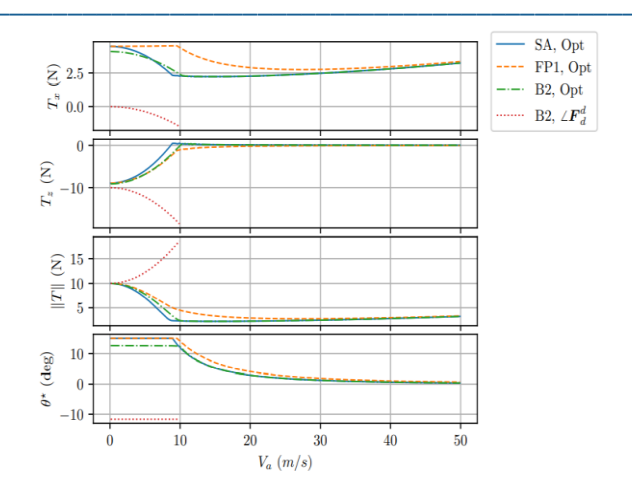


Figure. 11. Optimal thrust and pitch for increasing air speed at a flight path angles

Table 1. Waypoint used for spline comparison trajecto	t used for spline comparison trajector	comparison ti	spiine	ior	usea	ypoint	L. Wa	i abie 1	
---	--	---------------	--------	-----	------	--------	-------	----------	--

Waypoint	North	East	Down	Yaw
1	0	0	0	0
2	30	0	-5	0
3	50	0	-10	0
4	70	-5	-10	-22
5	80	-20	-5	-60
6	80	-25	0	-90

The reference trajectories are shown in dashed lines in Fig. 12, but the actual trajectories are shown in solid lines there. 12 to 20 seconds, which is when a vehicle is slowing down and starts to descend, accounts for the most tracking error. The average thrust and position error for each spline type are shown in Table 2 The B-spline has the biggest position inaccuracy, but the average thrust is the lowest. Due to the B-spline curves shifting more smoothly from one point to the next, the B-spline has a lower thrust.

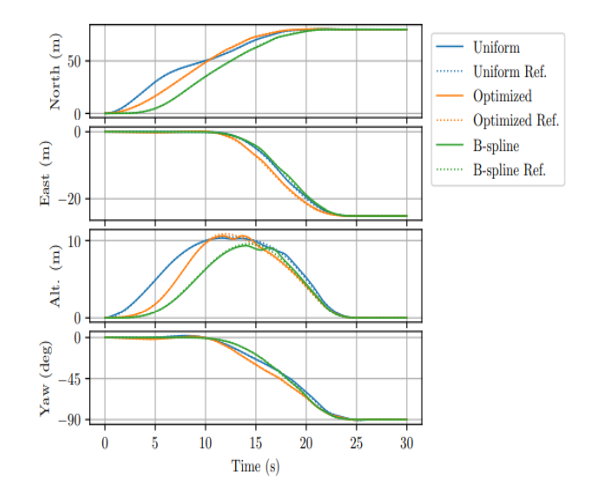


Figure. 12. Position and yaw reference and actual trajectories for B-spline, segment time optimized polynomial and uniform segment time polynomial trajectories.

Table 2. Spline comparison average position error and trust

Spline Type	Avg. Error	Avg. Thrust
B-spline	0.22	8.85
Optimized Polynomial	0.20	9.12
Uniform Polynomial	0.18	9.21

These three models are evaluated in Figure 14 truncated small-angle (SA), flat-plate (FP), and blended 2 (B2). The points at which the reference trajectory was generated. Figure 16 represents the schematic of the dynamic block of the proposed UAV method. A multi-rotor aircraft is travelling through a succession of points of interest. It takes us eight seconds to reach our final waypoint, which is eight seconds longer than we anticipated due to our waypoint tracking technique. This is due to the fact that the multirotor hits all of the way points in a sequential manner rather than passing through each one at the ideal time and speed. The output response is depicted in Figure 16.

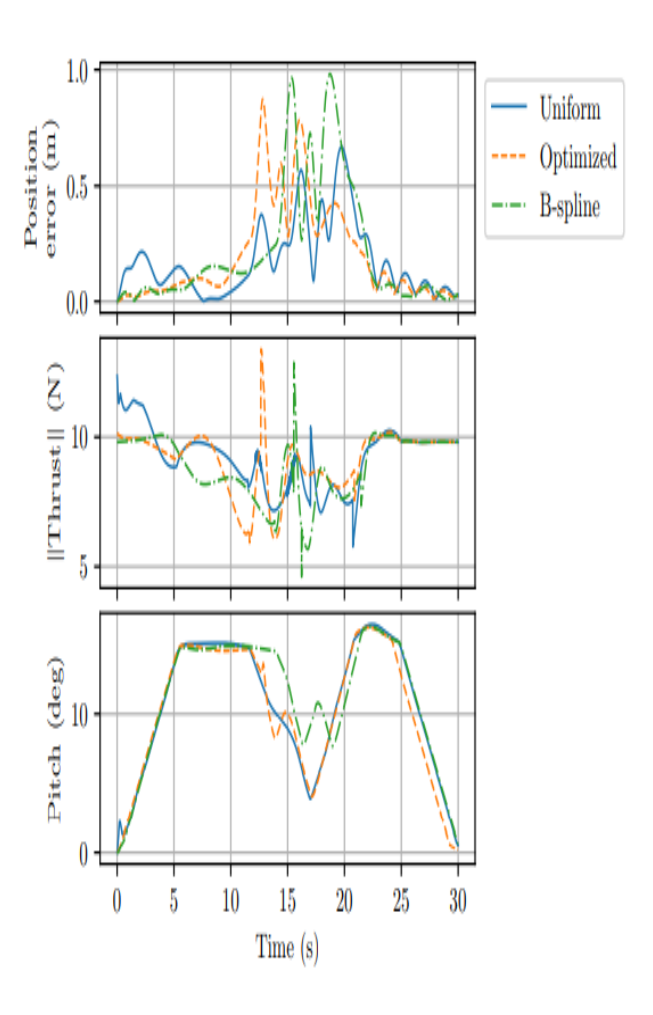


Figure. 13. Position error and pitch angle for B-spline, segment time optimized polynomial and uniform segment time polynomial trajectories.



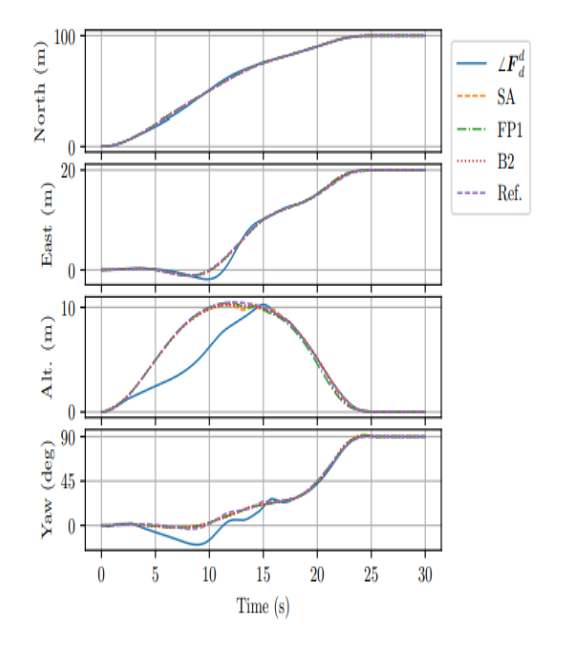


Figure. 14. Position error and yaw reference and actual trajectories for comparing the effect of using different angle - of- attack models in the pitch and thrust allocation.

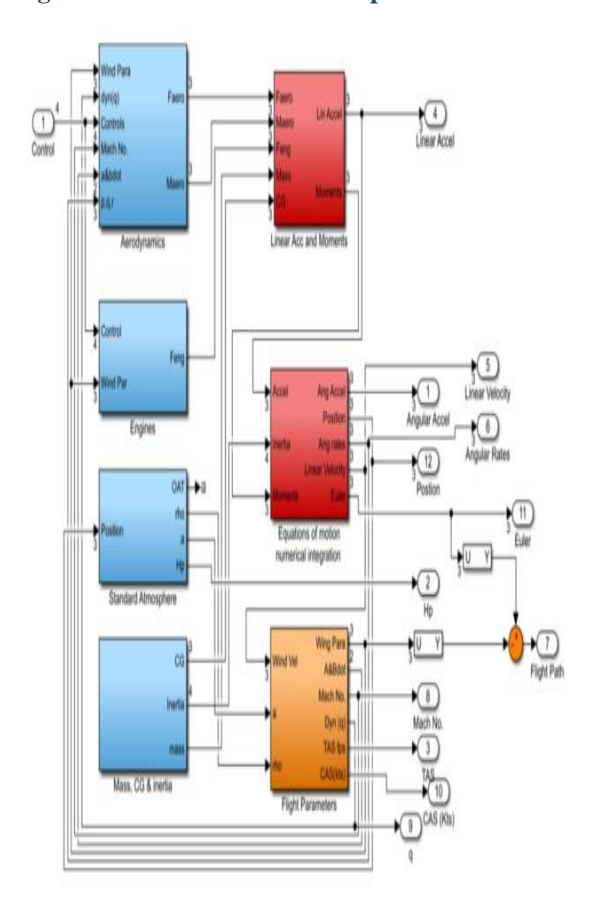


Figure. 15. Dynamic Block diagram of UAV

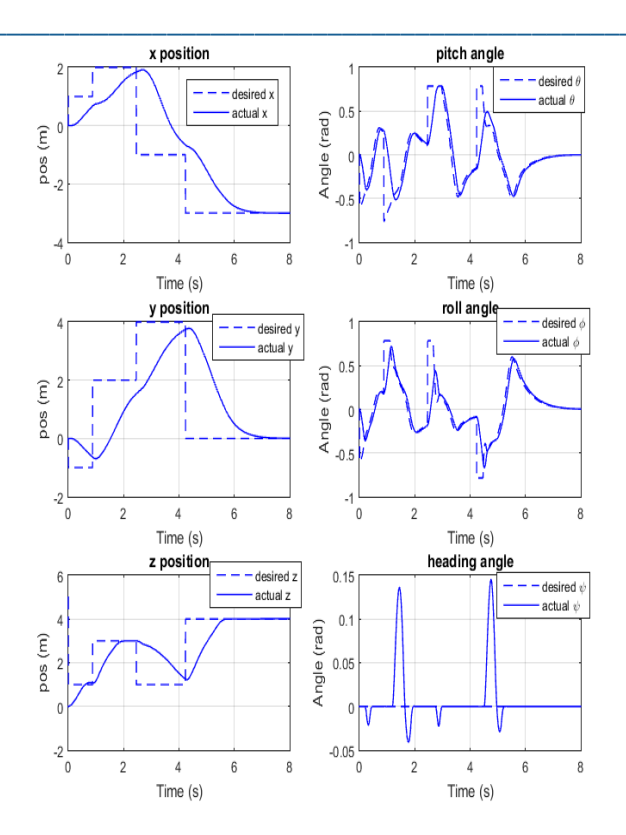


Figure. 16: Output Response of the Proposed Method

The comparison between the proposed and existing controllers is shown from the figure 17 to 20.

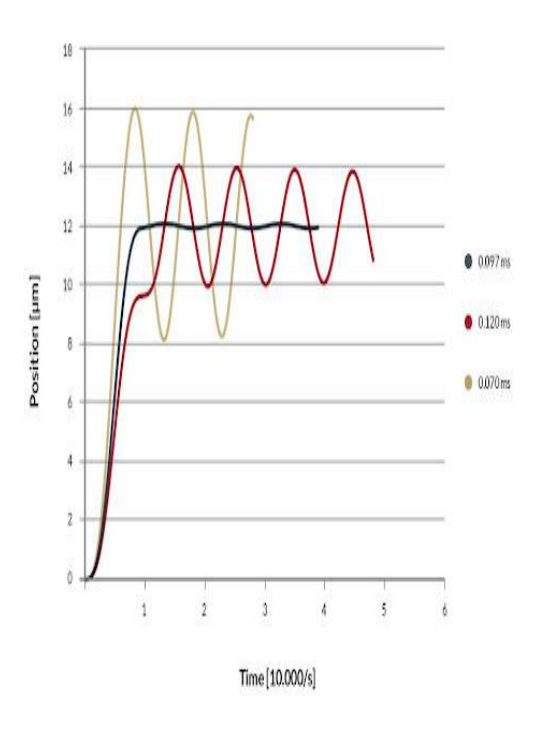


Figure. 17: Altitude step response for proposed and existing system

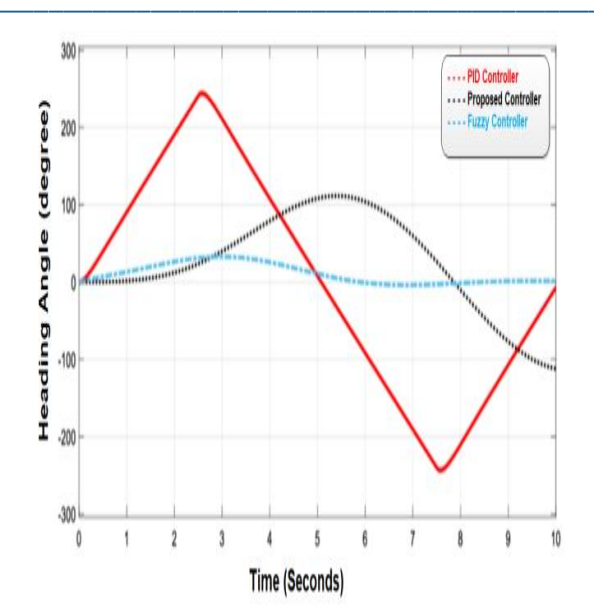


Figure. 18: Heading Step response for proposed and existing controller

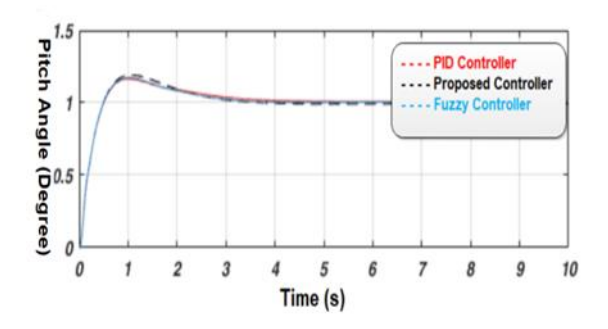


Figure. 19: Pitch angle response for proposed and existing controller

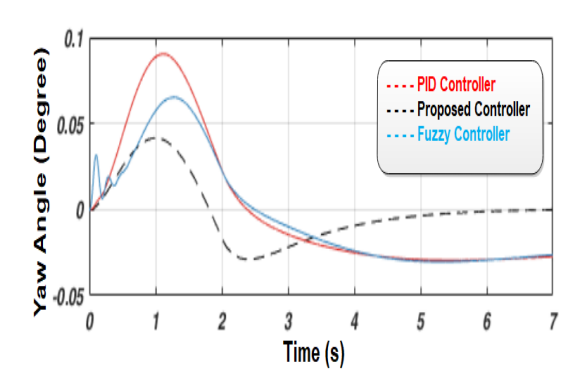


Figure. 20: YAW angle response for Proposed and existing controller

5. CONCLUSION

With the help of a controller that allows trajectory tracking along a position and yaw trajectory, fixed-wing unmanned aerial vehicles (UAVs) can now be integrated into current architectures for vision-based navigation and planning, which were originally designed for multirotor unmanned aerial vehicles. Furthermore, we will describe how to plan smooth trajectories by utilizing piecewise polynomial splines and B-splines. As proven by our simulation results, the proposed control approach is capable of tracking trajectories with high accuracy while using only a little amount of computing resources. The Pitch and Thrust Allocation Scheme described is based on static aerodynamic parameters, which limits its ability to control modelling mistakes or respond to changing flight

conditions in real time. In order to address this issue, model-free techniques such as extreme-seeking control, which may be used to identify the optimal pitch for a given energy-based goal function, could be examined in future research. Commercial jet aircraft have been simulated using a method that is similar to this one, in which the gradient of the efficiency function is computed using the longitudinal aerodynamic disturbances that the vehicle encounters.

Funding Statement: The author(s) received no specific funding for this study.

Conflicts of Interest: The authors declare that they have no conflicts of interest to report regarding the present study.

REFERENCES

- 1. Visintini, A., Perera, T.D.P., and Jayakody, D.N.K (2021), "3-D Trajectory Optimization for Fixed-Wing UAV-Enabled Wireless Network", *IEEE Access*, vol. 9, pp. 35045-35056.
- 2. Chen, P., Zhang, G., Guan, T., Yuan, M. and Shen, J (2021), "The Motion Controller Based on Neural Network S-Plane Model for Fixed-Wing UAVs", *IEEE Access*, vol. 9, pp. 93927-93936.
- 3. Xue, W., Qi, J., Shao, G., Xiao, Z., Zhang, Y. and Zhong, P (2021), "Low-Rank Approximation and Multiple Sparse Constraint Modeling for Infrared Low-Flying Fixed-Wing UAV Detection", *IEEE Journal of Selected Topics in Applied Earth Observations and Remote Sensing*, vol. 14, pp.4150-4166.
- 4. Bornebusch, M.F., and Johansen, T.A (2021), "Autonomous Recovery of a Fixed-Wing UAV Using a Line Suspended Between Two Multirotor UAVs", *IEEE Transactions on Aerospace and Electronic Systems*, vol. 57, no. 1, pp. 90-104.
- 5. Lee, M. and Lee, D. (2021), "A Distributed Two-Layer Framework for Teleoperated Platooning of Fixed-Wing UAVs via Decomposition and Backstepping", *IEEE Robotics and Automation Letters*, vol. 6, no. 2, pp. 3655-3662.
- 6. Umamaheswari, K., Prabhakar, G., Viji, K., Thanapal, P. (2021), "ANFIS PD Plus I Control On Simscape Model of Nonlinear Physical System", *Control Engineering and Applied Informatics, vol. 23, no. 1*, pp. 50-59.
- 7. Zhang, J. and Yan, J (2021), "A Novel Control Approach for Flight-Stability of Fixed-Wing UAV Formation with Wind Field," *IEEE Systems Journal*, vol. 15, no. 2, pp. 3655-3662.
- 8. Liu, J., Zhang, H., Sheng, M., Su, Y., Chen, S. and Li, J (2021), "High Altitude Air-to-Ground Channel Modeling for Fixed-Wing UAV Mounted Aerial Base Stations", *IEEE Wireless Communications Letters*, vol. 10, no.2, pp. 330-334.
- Qiu, C., Wei, Z., Feng, Z. and Zhang, P. (2020), "Backhaul-Aware Trajectory Optimization of Fixed-Wing UAV-Mounted Base Station for Continuous Available Wireless Service", *IEEE Access*, vol.8, pp. 60940-60950.
- 10. Borup, K.T., Stovner, B.N., Fossenand, T.I., Johansen, T.A. (2020), "Kalman Filters for Air Data System Bias Correction for a Fixed-Wing UAV," *IEEE Transactions on Control Systems Technology*", vol. 28, no.6, pp. 2164-2176.
- 11. Song, K., Zhang, J., Ji, Z., Jiang, J. and Li, C. (2020), "Energy-Efficiency for IoT System with Cache-Enabled Fixed-Wing UAV Relay," *IEEE Access*, vol.8, pp. 117503-117512.
- 12. Borup, K.T., Fossenand, T.I., Johansen, T.A. (2020), "A Machine Learning Approach for Estimating Air Data Parameters of Small Fixed-Wing UAVs Using Distributed Pressure Sensors," *IEEE Transactions on Aerospace and Electronic Systems*, vol. 56, no.3, pp. 2157-2173.
- 13. Mahfouz, M., Hafez, A.T., Azzam, A., Ashry, M., and Elnashar, G. (2020), "Formation Reconfiguration in Dynamic Obstacle Loaded Environment via Backstepping Approach", in *Proc.12th International Conference on Electrical Engineering (ICEENG): IEEE*, pp. 441-446.

- 14. Youn, W., Rhudy, M.B., Cho, A., and Myung, H. (2020), "Fuzzy Adaptive Attitude Estimation for a Fixed-Wing UAV with a Virtual SSA Sensor during a GPS Outage", *IEEE Sensors Journal*, vol. 20, no.3, pp. 1456-1472.
- 15. Ramamorrthy, M.L., Selvaperumal, S. and Prabhakar, G. (2022), "Self-Balancing Vehicle Based on Adaptive Neuro-Fuzzy Inference System", *Intelligent Automation and Soft Computing*, vol. 34, no. 1, pp. 485-497.
- 16. Liu, J., Sheng, M., Lyu, R., Shi, Y. and Li, J. (2020), "Access Points in the Air: Modeling and Optimization of Fixed-Wing UAV Network", *IEEE Journal on Selected Areas in Communications*, vol. 38, no.12, pp. 2824-2835.
- 17. Mitikiri, Y. and Mohseni, K. (2019), "Globally Stable Attitude Control of a Fixed-Wing Rudderless UAV Using Subspace Projection", *IEEE Robotics and Automation Letters*, vol. 4, no.2, pp. 1395-1401.
- 18. Yang, J., Wang, X. S. Baldi, S. Singh and S. Farì (2019), "A software-in-the-loop implementation of adaptive formation control for fixed-wing UAVs", *IEEE/CAA Journal of Automatica Sinica*, vol. 6, no.5, pp. 1230-1239.
- 19. Arya, J.S.R., Rao, S. and Datta guru, B (2019), "Effect of Asymmetric Control Constraints on Fixed-Wing UAV Trajectories", *IEEE Transactions on Aerospace and Electronic Systems*, vol. 55, no.3, pp. 1407-1419.
- 20. Min, Z., Chenming, Z. and Kun, H. (2019), "Fixed-wing UAV guidance law for ground target over-flight tracking", *Journal of Systems Engineering and Electronics*, vol. 30, no.2, pp. 384-392.
- 21. Mobarez, E.N., Sarhan, A. and Ashry, M. (2019), "Fractional order PID Based on a Single Artificial Neural Network Algorithm for Fixed wing UAVs", in *Proc.15th International Computer Engineering Conference (ICENCO): IEEE*, pp. 1-7.
- 22. Tang, Y., Xue, Z., Liu, X., Han, Q. and Tuo, X. (2019), "Leader-Following Consensus Control for Multiple Fixed-Wing UAVs' Attitude System with Time Delays and External Disturbances," *IEEE Access*, vol.7, pp. 169773-169781.
- 23. Wang, H., Wang, J., Ding, G., Chen, J., Gao, F. and Han, Z. (2019), "Completion Time Minimization with Path Planning for Fixed-Wing UAV Communications," *IEEE Transactions on* Wireless Communications, vol. 18, no.7, pp. 3485-3499.
- 24. Yang, L., Liu, Z., Wang, X. and Xu, Y. (2019), "An Optimized Image-Based Visual Servo Control for Fixed-Wing Unmanned Aerial Vehicle Target Tracking with Fixed Camera," *IEEE Access*, vol.7, pp. 68455-68468.
- 25. Tang, D., Shen, L. and Hu, T. (2019), "Online Camera-Gimbal-Odometry System Extrinsic Calibration for Fixed-Wing UAV Swarms," *IEEE Access*, vol.7, pp. 146903-146913.
- 26. Poksawat, P., Wang, L. and Mohamed, A. (2019), "Gain Scheduled Attitude Control of Fixed-Wing UAV With Automatic Controller Tuning," *IEEE Transactions on Control Systems Technology*, vol. 26, no.4, pp. 1192-1203.
- 27. Fusini, L., Fossenand, T.I., Johansen, T.A. (2018), "Nonlinear Observers for GNSS- and Camera-Aided Inertial Navigation of a Fixed-Wing UAV," *IEEE Transactions on Control Systems Technology*, vol. 26, no.5, pp. 1884-1891.
- 28. Zheng, Z., Jin, Z., Sun, L. and Zhu, M. (2017), "Adaptive Sliding Mode Relative Motion Control for Autonomous Carrier Landing of Fixed-Wing Unmanned Aerial Vehicles," *IEEE Access*, vol.5, pp. 5556-5565.